JCTC Journal of Chemical Theory and Computation

Electronic Structures of $AlGaN_2$ Nanotubes and AlN-GaN Nanotube Superlattice

Hui Pan,*,† Yuan Ping Feng,*,† and Jianyi Lin‡

Department of Physics, National University of Singapore, 2 Science Drive 2, Singapore 117542, and Institute of Chemical and Engineering Sciences, 1 Pesek Road, Jurong Island, Singapore 627833

Received November 14, 2007

Abstract: The electronic properties of single-wall $AlGaN_2$ nanotubes were investigated using first-principles calculations and generalized gradient approximation. All $AlGaN_2$ nanotubes considered are semiconductors, but their band structures depend on their chirality and size due to curvature effect and symmetry. The zigzag $AlGaN_2$ nanotubes are direct band gap semiconductors, while armchair $AlGaN_2$ nanotubes are indirect band gap semiconductors. The calculations on the electronic properties of AlN-GaN nanotubes superlattice show that the band gap engineering can be realized by changing the composition of the AlN-GaN nanotubes superlattice.

Introduction

Nanotubes have attracted extensive attention for their intriguing and potentially useful structural, electrical, and mechanical properties since the discovery of carbon nanotube (CNT). Theoretically, a number of nanotubes, such as GaN,[1] BN,[2] WC,[3] BC_2N,[4] SiC,[5] and AlN[6] nanotubes, have been predicted. Experimentally, a variety of nanotubes, such as BN,[7–9] $B_xC_yN_z$,[10,11] and AlN,[12] have been successfully synthesized by various methods, such as pulsed laser deposition, chemical vapor deposition, and wet chemistry. Recently, M. Remskar classified the inorganic nanotube (NTs) into six groups, including the following: oxide NTs, transition-metal chalcogenide NTs, transition-metal halogenous NTs, mixed-phase and metal-doped NTs, carbon-, boron-, and silicon-based NTs, and metal NTs.[13] For example, R. Tenne et al. first reported the transition-metal chalcogenide NTs, WS_2, and MoS_2, in 1992[14] and 1995,[15] respectively, and the transition-metal halogenous NTs, $NiCl_2$, in 1998.[16] They also studied the mechanical property and Raman scattering of WS_2 NTs.[17,18] It is well-known that the electronic properties of nanotubes depend on the size (radius) and chirality of the nanotubes. For single-walled CNTs (SWCNTs), the band gap of semiconducting SWCNT is inversely proportional to its diameter.[19] As for BC_2N nanotube, recent calculations indicated that both its electronic and optical properties were size and chirality dependent.[4,20]

III−V compound semiconductors are important materials in device application. Theoretical calculations indicated that the band gap of AlN and GaN single-wall nanotubes can be controlled by varying the size and chirality,[1,7] suggesting the applicability to full color flat panel displays. Experimentally, a bulk ternary semiconductor ($Al_xGa_{1-x}N$) has been widely studied for its application in devices, such as quantum well devices.[21] Gudiksen et al. reported the compositionally modulated superlattice nanowires consisting of 2−21 layers of GaAs and GaP for nanoscale photonics and electronics.[22] The superlattices are created within the nanowires by repeated modulation of the vapor-phase semiconductor reactants during growth of the wires. Multielement nanotubes can be expected to provide more tenability to their physical properties and to meet requirements of various applications. To the best of our knowledge, theoretically, the ternary nanotube, including Al, Ga, and N, has not been studied. In this article, we investigate the chirality and size dependence of electronic properties of armchair and zigzag $AlGaN_2$ nanotubes. We

* Corresponding author e-mail: phyph@nus.edu.sg (H.P.); phyfyp@nus.edu.sg (Y.P.F.).

† National University of Singapore.

‡ Institute of Chemical and Engineering Sciences.

10.1021/ct7003116 CCC: $40.75
Published on Web 04/15/2008

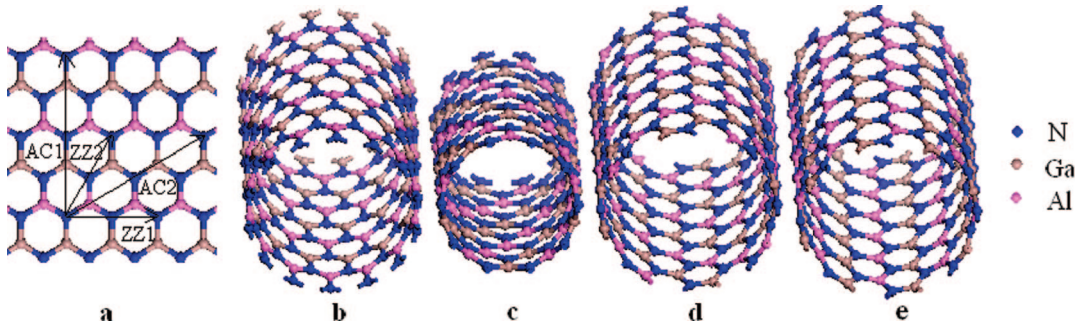

Figure 1. Atomic configurations of (a) the most stable $AlGaN_2$ sheet, (b) ZZ1 (14,0), (c) ZZ2 (0,5), (d) AC1 (8,8), and (e) AC2 (4,4) $AlGaN_2$ nanotubes. The Ga, Al, and N atoms are indicated by brown, pink, and blue spheres. The wrapping vectors of the four types of nanotubes are shown in (a).

also study possible band gap engineering by varying the composition of an AlN-GaN nanotube superlattice.

Calculation Details

We carried out first-principles calculation based on the density functional theory (DFT)[23] and the generalized gradient approximation (GGA).[24] The plane-wave based pseudopotential method and the CASTEP code were used in the study.[25] The ionic potentials are described by the ultrasoft nonlocal pseudopotential proposed by Vanderbilt.[26] The Monkhorst and Pack scheme of k point sampling was used for integration over the first Brillouin zone.[27] The Kohn−Sham energy functional is directly minimized using the conjugate-gradient method.[28] The convergence test indicated that an energy cutoff of 350 eV was sufficient for the calculations.

Compared to carbon nanotubes, there can be more than one type of zigzag or armchair $AlGaN_2$ nanotubes, depending on how an $AlGaN_2$ sheet is rolled up (Figure 1a). In this study, we considered two types of zigzag nanotubes: ZZ1 (n, 0) with $n = 5-16$ and ZZ2 (0, n) with $n = 3-8$, and two types of armchair nanotubes: AC1 (n, n) with $n = 3-11$ and AC2 (m, m) with $m = 2-5$, as shown in Figures 1b−e. In addition, AlN-GaN (6, 0) nanotube superlattices were studied. As the cell dimension in the direction of tube axis is different for different tube chirality, the k points used in the calculations are adjusted accordingly so that its density in the reciprocal space remains more or less the same, and the number of k points used in the calculations are 12 for ZZ1, 6 for ZZ2, 14 for AC1, and 6 for AC2 types of $AlGaN_2$ nanotubes, respectively. The k points used in the calculations of the AlN-GaN nanotube superlattices are 4. Good convergence was obtained with these parameters, and the total energy was converged to 2.0×10^{-5} eV/atom. A large supercell dimension with a wall−wall distance of 10 Å in the plane perpendicular to the tube axis was used to avoid interaction between the nanotube and its images in neighboring cells. The unit is periodic in the direction of the tube. The geometrically optimized nanotubes were used for band structure and optical property calculations.

As an indication of stability, the binding energy is estimated from the formula

$$E_b = |E_{tube} - n\mu_{Al} - n\mu_{Ga} - 2n\mu_N| \quad (1)$$

Table 1. Bond Lengths in Different Nanotubes after Geometry Optimization

nanotube	Al−N (Å)	Ga−N (Å)
AlN	1.81	
GaN		1.86
$AlGaN_2$	1.76	1.84
AlN-GaN	1.80	1.87

where E_{tube} is the energy of the $AlGaN_2$ nanotube. μ_{Al}, μ_{Ga}, and μ_N are chemical potentials of Al, Ga, and N atoms, respectively. n is the number of Al (or Ga) atoms in the nanotube.

Results and Discussion

A number of possible structures for planner $AlGaN_2$ were considered. Our total energy calculations indicated that the geometry with Ga and Al atoms separated by N atoms (Figure 1a) is most stable due to the lowest total energy. Other structures, such as the one with Ga atoms bonding to Al atoms, are less stable than that shown in Figure 1a due to the higher energy. The covalent bond lengths in the fully optimized structures are given in Table 1. For AlN and GaN nanotubes, the structure details are in good agreement with those of refs 1 and 6. The Al−N and Ga−N bond lengths in $AlGaN_2$ nanotubes are slightly less than those in AlN and GaN nanotubes.

Figure 2 shows the total energies per $AlGaN_2$ unit of the optimized $AlGaN_2$ nanotubes as a function of the tube diameter. The energy of the corresponding $AlGaN_2$ sheet is also shown for comparison. We can see that the total energies of all four types of $AlGaN_2$ nanotubes converge to that of the $AlGaN_2$ sheet as the diameter of the tubes increases. The energy difference between the tube and sheet decreases from 0.58 to 0.04 eV with the increase of the tube diameter. Furthermore, the total energies per $AlGaN_2$ unit of all four types of $AlGaN_2$ nanotubes with the same size are essentially the same, indicating that the strain energy of an $AlGaN_2$ nanotube, defined as the energy difference between the $AlGaN_2$ nanotube and the $AlGaN_2$ sheet, does not depend on its chirality. Figure 3 shows the binding energies of the optimized $AlGaN_2$ nanotubes as a function of the tube diameter. Similarly, at the same diameter, the binding energies of the four types of the $AlGaN_2$ nanotubes are almost equal, i.e., the binding energy of the $AlGaN_2$ nanotube

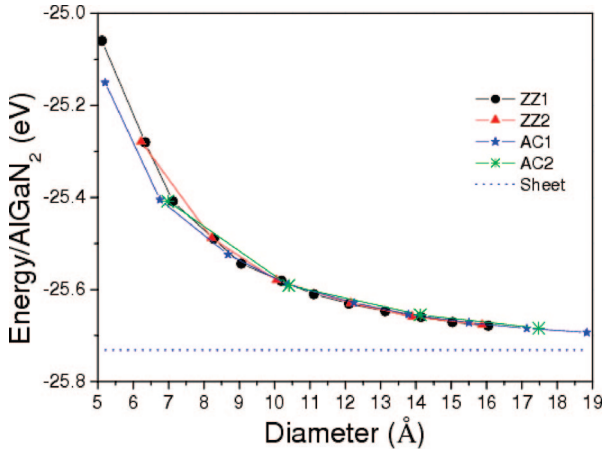

Figure 2. The total energies of AlGaN$_2$ nanotubes as a function of the diameter and a AlGaN$_2$ sheet.

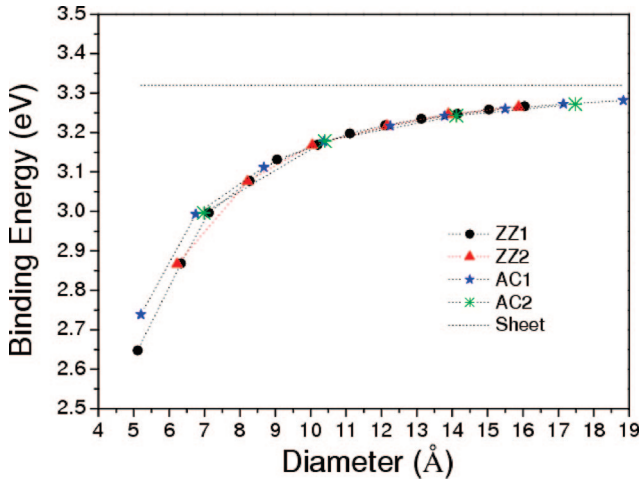

Figure 3. The binding energies of AlGaN$_2$ nanotubes as a function of the diameter and a AlGaN$_2$ sheet.

is chirality-independent. However, the binding energy of the AlGaN$_2$ nanotube is size-dependent due to the curvature effect. The binding energy increases with the increase of the diameter, indicating the AlGaN$_2$ nanotubes with larger diameter are more stable than those with smaller diameter. Therefore, from the energy point of view, all four types of AlGaN$_2$ nanotubes may be produced experimentally, although it is easier to grow AlGaN$_2$ nanotubes with larger diameters due to lower strain energy and higher binding energy.

Figure 4 shows the variation of the calculated GGA band gaps of various AlGaN$_2$ nanotubes with the diameter of the tubes. First of all, all AlGaN$_2$ nanotubes considered are semiconductors and the band gap of AlGaN$_2$ nanotube depends on its diameter and chirality. The band gap increases with an increase of diameter and converges to that of the AlGaN$_2$ sheet (2.87 eV) when the diameter of the tube becomes very large. The relatively smaller band gaps for the AlGaN$_2$ nanotubes with smaller diameters can be attributed to the curvature-induced strong hybridization effect. For nanotubes with the same diameter, the AC1 nanotubes have a slightly larger band gap. The band gaps of the AlGaN$_2$ nanotube are generally less than those of AlN and GaN nanotubes.[1,6] And the band gaps of the AlGaN$_2$

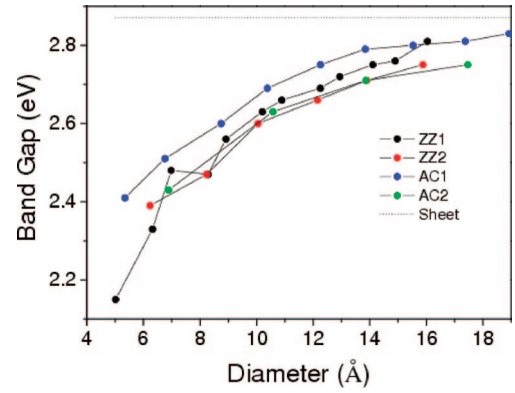

Figure 4. Band gaps of the AlGaN$_2$ nanotubes and the AlGaN$_2$ sheet are shown as functions of their diameters.

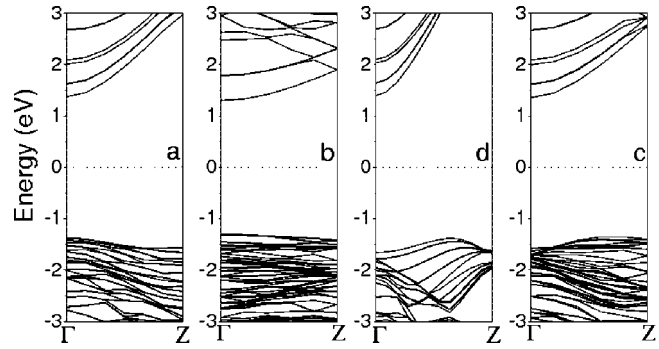

Figure 5. Calculated band structures of (a) ZZ1 (14, 0), (b) ZZ2 (0, 5), (c) AC1 (8, 8), and (d) AC2 (4, 4). The insets show the electron density of the highest valence energy level.

nanotubes are less than those of bulk wurtzite Al$_x$Ga$_{1-x}$N ($0 \leq x \leq 1$) alloys, which have tunable direct band gaps between 3.4 and 6.1 eV, depending on the Al content. Therefore, these AlGaN$_2$ nanotubes can be recognized as important semiconductors for optoelectronic device applications over the visible spectral range.

The representative band structures of the four types of AlGaN$_2$ nanotubes near the Fermi level were demonstrated in Figure 5. All zigzag (ZZ1 and ZZ2) nanotubes are direct band gap semiconductors with the bottom of the conduction energy level and the top of the valence energy level located at the Brillouin zone center (Γ) (Figure 5a,b). On the contrary, all armchair (AC1 and AC2) nanotubes are indirect gap semiconductors, with the bottom of the conduction energy level located at the Γ point but the top of the valence energy level at $\sim^2/_3$ along the ΓZ direction (Figure 4c,d). Analysis of electron densities corresponding to the top valence band of the zigzag AlGaN$_2$ nanotube shows that the top valence band consists of *p* orbitals of the nitrogen atoms next to Al atoms in the direction of the tube axis. These *p* orbitals are normal to the tube surface (Figure 6a). For the armchair AlGaN$_2$ nanotube, the valence top level is attributed to similar *p* orbitals of all nitrogen atoms (Figure 6b). These observations indicate that the electronic properties of the AlGaN$_2$ nanotubes are chirality-dependent. And the valence top levels in AlGaN$_2$ nanotubes with different chirality are attributed to the *p* orbitals from different atoms due to the difference in symmetry.

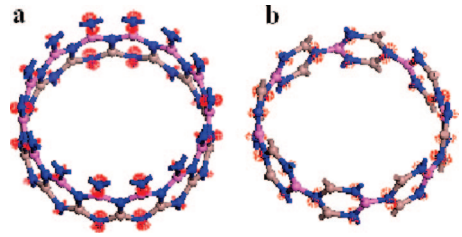

Figure 6. The electron density of the valence top level of (a) ZZ1 (14, 0) and (b) AC1 (8, 8).

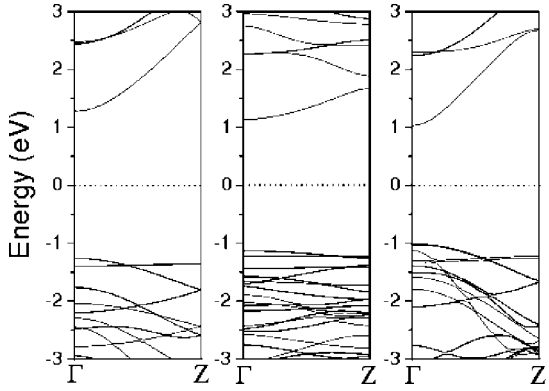

Figure 7. Calculated band structures of (a) AlN (6, 0) nanotube, AlN-GaN (6, 0) nanotube superlattice, and (c) GaN (6, 0) nanotube.

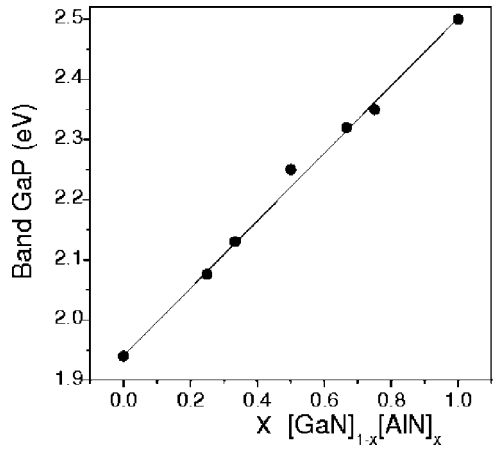

Figure 8. Band gap of $[AlN\ (6, 0)]_x[GaN\ (6, 0)]_{1-x}$ nanotube superlattice as a function of the *x*.

The AlN-GaN nanotube superlattices consists of alternating AlN (6, 0) and GaN (6, 0) segments of different lengths, i.e. $[AlN\ (6, 0)]_x[GaN\ (6, 0)]_{1-x}$. Restuls of our calculations indicated that Al−N and Ga−N bond lengths in the superlattice are very close to those in separate AlN and GaN nanotubes (Table 1). The band structures of AlN (6, 0) nanotube, AlN-GaN nanotube superlattice with $x = 0.5$ and a GaN (6, 0) nanotube, illustrated that they are direct semiconductors (Figure 7). The band gap of the $[AlN\ (6, 0)]_{0.5}[GaN\ (6, 0)]_{0.5}$ nanotube (2.25 eV) is slightly smaller than that of $AlGaN_2$ (6, 0) nanotube (2.33 eV), which is about the average of the band gaps of the AlN (6, 0) nanotube ($E_{AlN} = 2.50$ eV) and the GaN (6, 0) nanotube ($E_{GaN} = 1.94$ eV). The p orbitals normal to the tube surface of the nitrogen atoms at the interface of the junction contribute to the top valence band by the analysis of electron densities of the top valence band of AlN-GaN nanotube superlattice. A number of $[AlN\ (6, 0)]_x[GaN\ (6, 0)]_{1-x}$ nanotube superlattice with different *x* were investigated. Figure 8 shows the change of the band gap of the AlN-GaN superlattices (E_s) with *x*. The linear dependence of E_s on the *x* implies that E_s for a $[AlN\ (6, 0)]_x[GaN\ (6, 0)]_{1-x}$ nanotube superlattice with an arbitrary *x* can be estimated based on the simple linear interpolation, $E_s = xE_{GaN} + (1-x)E_{AlN}$.

Conclusions

In summary, first-principles calculations on the electronic properties of single-wall $AlGaN_2$ nanotubes indicated that the electronic properties of the $AlGaN_2$ nanotubes are size and chirality dependent due to the curvature effect and symmetry. The band gap of the $AlGaN_2$ nanotube increases with increasing size and converges to that of the planner $AlGaN_2$. Our calculations also predicted that the band gap of $[AlN\ (6, 0)]_x[GaN\ (6, 0)]_{1-x}$ nanotube superlattice can be engineered by changing the composition. Although the well-known fact that DFT/GGA underestimates the band gap of semiconductors, the dependence of the electronic properties of the nanotubes on their size and chirality are valid. The theoretical results should be confirmed experimentally.

References

(1) Lee, S. M.; Lee, Y. H.; Hwang, Y. G.; Elsner, J.; Porezag, D.; Frauenheim, T. Stability and Electronic Structure of GaN Nanotubes From Density-Functional Calculations. *Phys. Rev. B* **1999**, *60*, 7788.

(2) Rubio, A.; Corkill, J. L.; Cohen, M. L. Theory of Graphitic Boron Nitride Nanotubes. *Phys. Rev. B* **1994**, *49*, 5081.

(3) Pan, H.; Feng, Y. P.; Lin, J. Hydrogen Adsorption by Tungsten Carbide Nanotube. *Appl. Phys. Lett.* **2007**, *90*, 223104.

(4) Pan, H.; Feng, Y. P.; Lin, J. Ab Initio Study of Single-wall BC_2N Nanotubes. *Phys. Rev. B* **2006**, *74*, 045409.

(5) Menon, M.; Richter, E.; Mavrandonakis, A.; Froudakis, G.; Andriotis, A. N. Structure and Stability of SiC Nanotubes. *Phys. Rev. B* **2004**, *69*, 115322.

(6) Zhao, M.; Xia, Y.; Zhang, D.; Mei, L. Stability and Electronic Structure of AlN Nanotubes. *Phys. Rev. B* **2003**, *68*, 235415.

(7) Zhou, Z.; Zhao, J.; Chen, Z.; Gao, X.; Lu, J. P.; Schleyer, P. V. R.; Yang, C.-K. True Nanocable Assemblies with Insulating BN Nanotube Sheaths and Conducting Cu Nanowire Cores. *J. Phys. Chem. B* **2006**, *110*, 2529.

(8) Tang, C.; Bando, Y.; Huang, Y.; Yue, S.; Gu, C.; Xu, F.; Golberg, D. Fluorination and Electrical Conductivity of BN Nanotubes. *J. Am. Chem. Soc.* **2005**, *127*, 6552.

(9) Tang, C.; Bando, Y.; Ding, X.; Qi, S.; Golberg, D. Catalyzed Collapse and Enhanced Hydrogen Storage of BN Nanotubes. *J. Am. Chem. Soc.* **2002**, *124*, 14550.

(10) Kim, S. Y.; Park, J.; Choi, H. C.; Ahn, J. P.; Hou, J. Q.; Kang, H. S. X-ray Photoelectron Spectroscopy and First Principles Calculation of BCN Nanotubes. *J. Am. Chem. Soc.* **2007**, *129*, 1705.

(11) Suenaga, K.; Colliex, C.; Demoncy, N.; Loiseau, A.; Pascard, H.; Willaime, F. Synthesis of Nanoparticles and Nanotubes with Well-Separated Layers of Boron Nitride and Carbon. *Science* **1997**, *278*, 653.

(12) Wu, Q.; Hu, Z.; Wang, X.; Lu, Y.; Chen, X.; Xu, H.; Chen, Y. Synthesis and Characterization of Faceted Hexagonal Aluminum Nitride Nanotubes. *J. Am. Chem. Soc.* **2003**, *125*, 10176.

(13) Remskar, M. Inorganic Nanotubes. *Adv. Mater.* **2004**, *16*, 1497.

(14) Tenne, R.; Margulis, L.; Genut, M.; Hodes, G. Polyhedral and Cylindrical Structures of Tungsten Disulphide. *Nature* **1992**, *360*, 444.

(15) Feldman, Y.; Wasserman, E.; Srolovitz, D. J.; Tenne, R. High-Rate, Gas-Phase Growth of MoS_2 Nested Inorganic Fullerenes and Nanotubes. *Science* **1995**, *267*, 222.

(16) Hacohen, M. E.; Grunbaum, E.; Tenne, R.; Sloan, J.; Hutchison, J. L. Cage Structures and Nanotubes of $NiCl_2$. *Nature* **1998**, *395*, 336.

(17) Kaplan-Ashiri, I.; Cohen, S. R.; Gartsman, K.; Ivanovskaya, V.; Heine, T.; Seifert, G.; Wiesel, I.; Wagner, H. D.; Tenne, R. On the Mechanical Behavior of WS_2 Nanotubes Under Axial Tension and Compression. *PNAS* **2006**, *103*, 523.

(18) Rafailov, P. M.; Thomsen, C.; Gartsman, K.; Kaplan-Ashiri, I.; Tenne, R. Orientation Dependence of The Polarizability of An Individual WS_2 Nanotube by Resonant Raman Spectroscopy. *Phys. Rev. B* **2005**, *72*, 205436.

(19) Hamada, N.; Sawada, S.; Oshiyama, A. New One-dimensional Conductors: Graphitic Microtubules. *Phys. Rev. Lett.* **1992**, *68*, 1579.

(20) Pan, H.; Feng, Y. P.; Lin, J. First-principles Study of Optical Spectra of Single-wall BC_2N Nanotubes. *Phys. Rev. B* **2006**, *73*, 035420.

(21) Shubina, T. V.; Toropov, A. A.; Jmerik, V. N.; Tkachman, M. G.; Lebedev, A. V.; Ratnikov, V. V.; Sitnikova, A. A.; Vekshin, V. A.; Ivanov, S. V.; Kopev, P. S.; Bigenwald, P.; Bergman, J. P.; Holtz, P. O.; Monemar, B. Intrinsic Electric Fields in N-polarity $GaN/Al_xGa_{1-x}N$ Quantum Wells with Inversion Domains. *Phys. Rev. B* **2003**, *67*, 195310.

(22) Gudiksen, M. S.; Lauhon, L. J.; Wang, J.; Smith, D. C.; Lieber, C. M. Growth of Nanowire Superlattice Structures for Nanoscale Photonics and Electronics. *Nature* **2002**, *415*, 617.

(23) Hohenberg, P.; Kohn, W. Inhomogeneous Electron Gas. *Phys. Rev.* **1964**, *136*, B864.

(24) Perdew, J. P.; Wang, Y. Accurate and Simple Analytic Representation of The Electron-gas Correlation Energy. *Phys. Rev. B* **1992**, *45*, 13244.

(25) Payne, M. C.; Teter, M. P.; Allan, D. C; Arias, T. A.; Joannopoulos, J. D. Iterative Minimization Techniques for ab initio Total-energy Calculations: Molecular Dynamics and Conjugate Gradients. *Rev. Modern Phys.* **1992**, *64*, 1045.

(26) Vanderbilt, D. Soft Self-consistent Pseudopotentials in A Generalized Eigenvalue Formalism. *Phys. Rev. B* **1990**, *41*, 7892.

(27) Monkhorst, H. J.; Pack, J. Special Points for Brillouin-zone Integrations. *Phys. Rev. B* **1976**, *13*, 5188.

(28) Teter, M. P.; Payne, M. C.; Allan, D. C. Solution of Schrödinger's Equation for Large Systems. *Phys. Rev. B* **1989**, *40*, 12255.

(29) Nepal, N.; Bedair, S. M.; El-Masry, N. A.; Lee, D. S.; Steckl, A. J.; Zavada, J. M. Correlation Between Compositional Fluctuation and Magnetic Properties of Tm-doped AlGaN Alloys. *Appl. Phys. Lett.* **2007**, *91*, 222503.

CT7003116